J Mater Sci: Mater Med (2009) 20:215–222
DOI 10.1007/s10856-008-3562-7

Corrosion resistance evaluation of a Ca- and P-based bioceramic thin coating in Ti-6Al-4V

Paulo G. Coelho · Sérgio Luiz de Assis · Isolda Costa · Van P. Thompson

Received: 3 May 2008 / Accepted: 25 July 2008 / Published online: 25 August 2008

Abstract The objective of this study was to physico/chemically characterize and determine the corrosion resistance of a Calcium–Phosphate (Ca–P) based bioceramic thin coating processed by a sputtering process on titanium alloy (Ti-6Al-4V). The samples utilized in this study were uncoated and coated disks of 10 mm diameter by 3 mm thickness. The coating was characterized by SEM, XPS + ion beam milling (IBM), thin-film mode XRD, and atomic force microscope (AFM) ($n = 3$). Coated and uncoated Ti-6Al-4V disk surfaces were tested in Phosphate Buffered Saline (PBS) at 25°C through an area of 0.79 cm^2. A three-electrode cell set-up was used with a saturated calomel electrode (SCE) and a platinum wire as reference and counter electrodes. After 3, 17, and 25 days of immersion, electrochemical impedance spectroscopy (EIS) experiments were performed ($n = 3$). The EIS tests were carried out in potentiostatic mode at the open circuit potential (OCP). The frequency range considered was from 100 kHz to 10 mHz, using 10 mV root mean square as the amplitude of the perturbation signal. A potentiodynamic polarization scan using a frequency response analyzer potentiostat, was acquired following 3 days of immersion in PBS. The potentiodynamic polarization scans ($n = 3$) were carried out with a scan rate of 1 mV/s ranging from −0.8V(SCE) to 3.0V(SCE). Results: The physico/chemical characterization showed an amorphous Ca- and P-based coating of ~400–700 nm thickness with Ca–P nanometer size particles embedded in a Ca–P matrix. The Bode phase angle diagrams showed highly capacitive results at low and medium frequencies for both surfaces tested. The polarization curves showed low current densities at the corrosion potential (E_{corr}), in the order of 10^{-8}A/cm^2, typical of passive materials with protective surface films. Coated sample current densities were comparable to the uncoated samples. Conclusion: Coated and uncoated samples were stable in the test solution with a protective film maintained throughout the 25 day immersion test period.

P. G. Coelho (✉) · V. P. Thompson
Department of Biomaterials and Biomimetics, New York University College of Dentistry, 345 East 24th Street, Room 804S, New York, NY 10100, USA
e-mail: pgcoelho@nyu.edu

S. L. de Assis · I. Costa
Materials Science and Technology Centre, Energy and Nuclear Research Institute (IPEN/CNEN-SP), Av. Prof. Lineu Prestes, 2242, 05508-900 Sao Paulo, SP, Brazil

1 Introduction

The short- and long-term success of metallic implant devices utilized for orthopedic and dental rehabilitation is dependent on their ability to maintain physical and chemical properties in the dynamic physiologic environment. Titanium alloys have the inherent ability to spontaneously develop a protective oxide surface layer which coupled with outstanding mechanical properties, has lead to wide usage in implantable musculo-skeletal devices [1].

Since the implant surface is the first to interact with the host, its biocompatible and osteoconductive properties are key for the modulation of the biofluid, cellular, and tissue level interactions that modulate osseointegration [2].

Several surface engineering methods have been used in an attempt to increase the biocompatibility and osteoconductivity of titanium implants. Among them, surface texturing processes have been shown to hasten the biologic response and biomechanical fixation of implants compared to as-machined surfaces [3, 4]. However, texturization of

titanium alloy surfaces may involve processes that increase the levels of alloying elements at the surface and also result in an increase in surface area both potentially increasing ion release. Accumulation of metal ions in the peri-implant tissues has been speculated to result in adverse effects at both cellular and tissue levels [5–7]. Coating metallic implants with bioactive ceramics to decrease ion released has been attempted to increase biocompatibility and provide osteoconductive properties [1, 8–10].

At early implantation times, plasma sprayed hydroxyapatite (PSHA) coated implants showed enhanced in vivo bone-to-bioceramic bonding, and bone-to-implant contact [8–14]. However, these coatings may be partially dissolved/resorbed after long periods in function [10–12, 14]. In addition, PSHA manufactured implant coatings normally rely on mechanical interlocking between a grit-blasted or etched metallic surfaces and the ceramic-like PSHA material to maintain physical integrity during placement and function [9]. This specific interface between the bulk metal, metal oxide, and bioceramic coating has been regarded by some as a weak link, where failures during insertion or after osseointegration have been reported to occur from loss of adhesion [8, 9, 13].

In an attempt to improve on these short comings, thin-film bioceramic coatings have been developed for implant surfaces through various techniques [9]. These techniques often apply substantially thinner coatings compared to PSHA coatings [9]. Desirable features of thin-film coatings include controlled composition and thickness plus enhanced adhesion to the metallic substrate while maintaining substrate surface roughness [9–12, 15, 16]. Controlled composition and thickness achievable through thin film processes also influence coating dissolution in vivo [10], thereby potentially affecting the device's osteoconductivity at early implantation times [15]. Dissolution may also expose the metallic substrate after surgical placement. Therefore, the possibility of having close bone contact with the implant metallic substrate after coating dissolution may be an attractive feature of thin-films. This close contact could avoid potential less desirable interfaces between bone, bioceramic, surface oxides, and implant substrate. From a theoretic standpoint, the absence of such interfaces is favorable for long-term implant anchorage [10, 12, 15].

From a biocompatibility and biomechanical point of view, thin coatings may present advantages over thicker PSHA coatings [10]. However, their morphology, reduced dimensions and process dependent composition may result in substantially different electrochemical behavior while interacting with bone in the physiologic environment.

The objective of this study was to physico/chemically characterize and determine the corrosion resistance of a Ca- and P-based bioceramic thin coating sputtered on titanium alloy (Ti-6Al-4V) using electrochemical methods.

2 Materials and methods

As-machined Ti-6Al-4V disks of ~10 mm diameter and 3 mm thickness were utilized as substrates. The thin Ca–P coatings were produced by a single ion beam sputtering process [10, 15]. Rough evacuation was performed using a mechanical pump and high vacuum (6×10^{-6} torr) was attained through a cryopump. Prior to deposition, the disk surfaces were cleaned with an ion-beam utilizing 120V and 2 A, and the chamber was backfilled with oxygen to 2×10^{-5} torr. The sputtering target was a PSHA (~35% crystalline, Bicon, LLC, Boston, MA) coated Ti-6Al-4V disk of 100 mm diameter and 20 mm thickness in a copper holder. The PSHA coating on the sputtering target had a thickness of ~100 μm. The sputtering parameters were 120 V and 5 mA, and the target coating thickness for the disks was 500 nm.

For coating thickness measurement, three disks of 25 mm diameter and 3 mm thickness were subjected to the same deposition parameters utilized for the implants.

2.1 Coating physico/chemical characterization

Three disks were used for the series of analytical instrumentation employed for surface physico/chemical characterization.

Field Emission scanning electron microscopy (FE-SEM) (Phillips FEI XL30 FEG-SEM, Eindhoven, The Netherlands) was performed at various magnifications under an acceleration voltage of 15 KeV. To evaluate surface microtexture, 20 × 20 μm scans in different regions of the disks were acquired by an atomic force microscope (AFM) in contact model (Nanoscope IIIa Multimode System, Digital Instruments, Santa Barbara, CA). A scanner with a maximum 125 μm horizontal and 5 μm vertical range, and a 200 nm Si_3N_4 cantilever tip with a force constant of 0.12 N/m was used.

Surface-specific chemical assessment was performed by inserting the disks into a vacuum transfer chamber and degassing it to 10^{-7} torr. The samples were then transferred under vacuum to a Kratos Axis 165 multitechnique XPS spectrometer (Kratos Analytical Inc., Chestnut Ridge, NY). Survey and high-resolution spectra were obtained using a 165 mm mean radius concentric hemispherical analyzer operated at constant pass energy of 160 eV for survey and 80 eV for high resolution scans. Survey scans were performed at various locations on the implant body. A built-in charge neutralizer was used when necessary to compensate for sample charge build up during XPS analysis. All spectra were referenced to the adventitious carbon C1 s peak position of 285.0 eV.

For coating thickness measurement, a combination of AFM and depth profiling by XPS and Ion Beam Milling

(IBM) was utilized. However, it was necessary to process additional coatings with a thickness of ~300 nm to facilitate calculation of the coating IBM etching rate. A portion of the deposited bioceramic was mechanically removed by means of a sharp instrument from the center of each disk to expose the metallic substrate. Subsequently, an AFM in contact mode was utilized for direct coating thickness determination (3 measurements per disk, with height measurements taken at the scratched region and regions >3 mm away from the scratch to avoid height distortion due to coating mechanical removal). Then depth profiling was conducted using a 4 keV Ar + ion sputter gun to etch the experimental disks surfaces at 5 min intervals and at each interval XPS high resolution scans were carried out and this process repeated until the base alloy components were detected. The approximate etching rate calculated for the coating was ~4 nm/min. The depth profiling procedure was completed on the three test disks at three different positions on the disk surface.

Coating crystallographic assessment was performed by Thin-Film Mode X-Ray Diffraction (TFXRD). The implants were scanned from 30 to 38 degrees two theta at 0.05 degrees step size (2 s time step), 45 KV accelerating voltage, and 40 mA current. The rationale for using this two theta range was due to the presence of an alpha-Ti peak at approximately 35.5 two theta degrees as well as known high intensity HA peaks (at 31 and 33 two theta degrees) and other Ca–P based phases commonly found in bioceramic coated implants [8, 17]. The peaks location/intensity versus two theta degree output was compared to theoretic crystallographic calculations for; alpha (HCP), beta (BCC), and other Ca–P based phases, as well as titanium.

2.2 Electrochemical tests

Prior to immersing into the testing electrolyte, the disks were degreased in an ultrasonic bath for 5 min, rinsed with deionized water, and then dried under a hot air stream. The coated and uncoated Ti-6Al-4V disk surfaces were then exposed to the electrolyte through an area of 0.79 cm^2. The electrolyte (test medium) used was a Phosphate Buffered Saline (PBS) (Table 1) at 25°C [18–20]. A three-electrode cell set-up was used with a saturated calomel electrode (SCE), a platinum wire as reference, and a counter electrode.

Table 1 Chemical composition of PBS solution [18–20]

Component	mg/l
NaCl	8.77
$Na_2HPO_4 \cdot 12H_2O$	3.58
KH_2PO_4	1.36
pH	7.2–7.4

Electrochemical impedance spectroscopy (EIS) experiments were performed after 3 days, 17 days, and 25 days of immersion. The EIS tests were carried out in potentiostatic mode at the open circuit potential (OCP). The frequency range considered was from 100 kHz to 10 mHz, using 10 mV root mean square as the amplitude of the perturbation signal, and an acquisition rate of 6 points per decade.

A potentiodynamic polarization scan using a frequency response analyzer (Gamry model EIS 300) coupled to a potentiostat PCI4/300, was acquired following 3 days of immersion in PBS. The potentiodynamic polarization scans were carried out with a scan rate of 1 mV/s ranging from −0.8 V (SCE) to 3.0 V (SCE). Both the EIS and polarization tests were carried out in triplicate in order to evaluate the results reproducibility.

3 Results and discussion

The FE-SEM at showed that thin bioceramic coatings fully covered the disk surface. High resolution imaging at higher magnifications showed that the coating morphology resembled a composite with nano particles embedded within a matrix (Fig. 1a). AFM analysis confirmed the

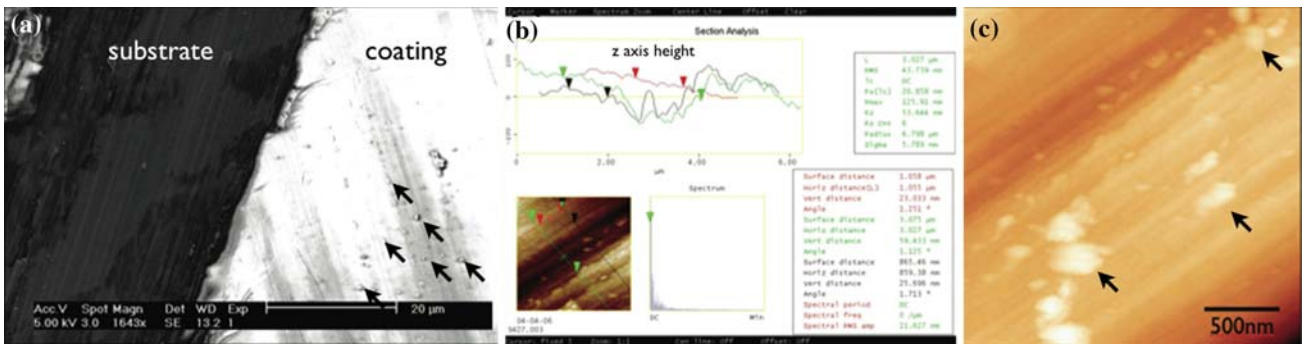

Fig. 1 (**a**) FE-SEM of a region where the thin coating was mechanically removed from the disk surface, showing that the high energy beam resulted in the deposition of particles (representatively depicted by arrows) ranging from a few to several hundred micrometers, supported by (**a**) FESEM and (**b** and **c**) direct contact AFM measurements. Note the z axis height differences in (**b**)

presence of bioceramic particles ranging from a few to several hundred nanometers in dimension (Fig. 1b, c).

The XPS survey analyses detected the presence of O, C, Ca, and P on the coating surfaces. The coating thickness assessment utilizing the experimentally derived coating etching rate [21] showed that coating thicknesses ranged from ~400 to 700 nm depending upon region. The elemental chemistry as a function of coating thickness is presented in Fig. 2a, and the Ca/P stoichiometry through the coating thickness presented in Fig. 2b. The variation in

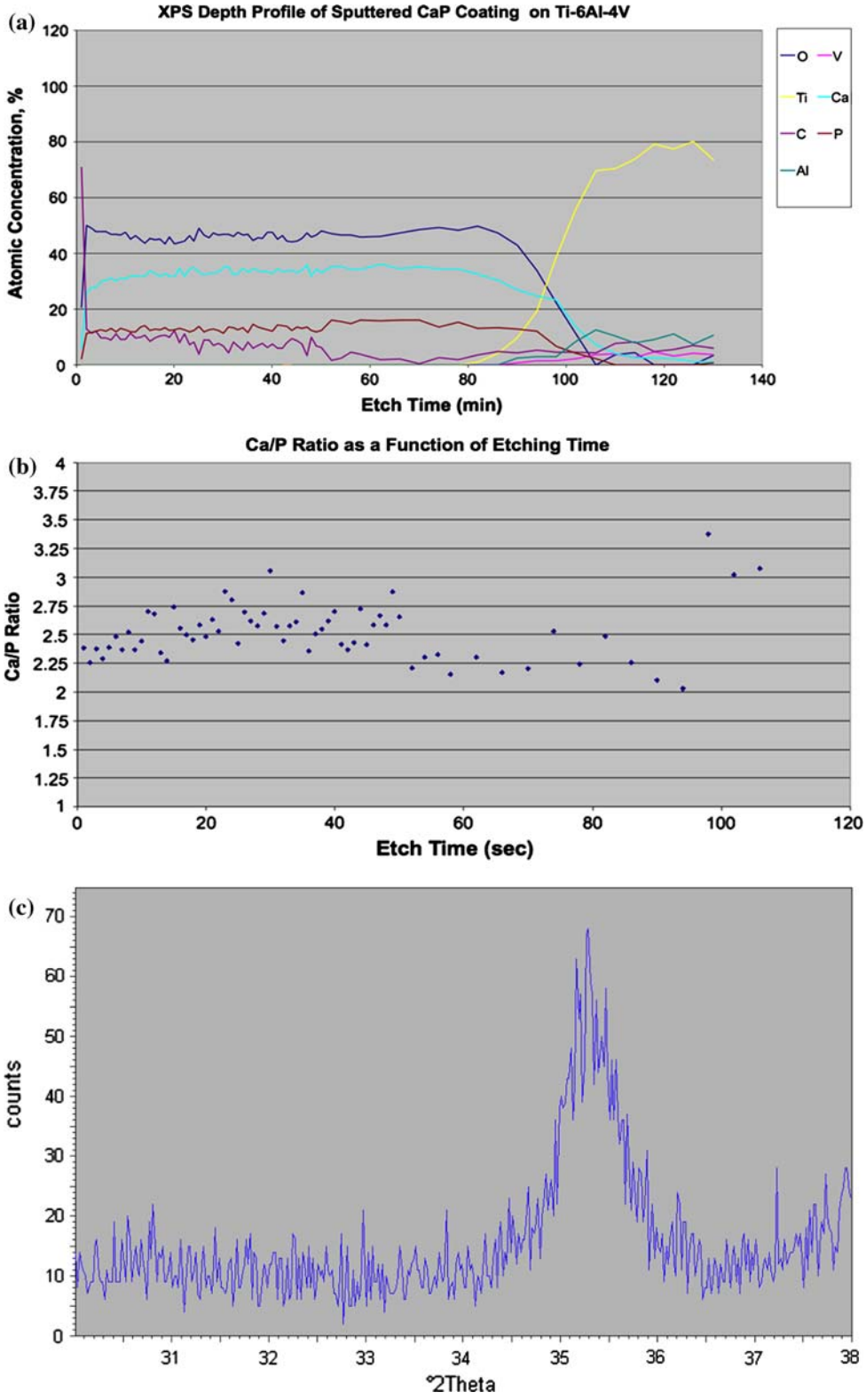

Fig. 2 (**a**) coating depth profile, (**b**) coating Ca/P ratio as a function of etch time, and (**c**) thin-film mode XRD spectrum showing a 2 theta peak associated to alpha Ti

Ca/P stoichiometry as a function of coating depth observed for the samples compared to crystalline HA (1.677) likely resulted from the multiphase composition and spatial distribution throughout the surface and depth of the PSHA target employed for coating processing, and also due to potential preferential deposition during coating fabrication [8, 9, 22, 23].

Despite the success reported in a clinical trial initiated in 1985 by Furlong and Osborn [24] for bioactive coatings of implant surfaces, the use of bioactive implant surfaces was not expanded in clinical practice due in part to potential limitations of such coatings. Concerns existed about inconsistent thicknesses and composition and a potential weak link at the interface between coating and implant substrate [1, 8–10, 25, 26]. Thus, extensive research over the last three decades has concentrated on coating process optimization and methods to improve the properties of the coating-implant substrate interface [3, 4, 14, 24, 26–32].

The coating micromorphology resembled a matrix embedded with nanometer range particles. This was thought to be the result of the high energy of the ion beam, which instead of removing the target components on an atomic scale only, removed the target material in a range of sizes including clusters of several hundred nanometers. The full surface coverage with thicknesses ranging from 400 to 700 nm obtained with the high energy beam sputtering process is projected as important for increasing the biocompatible and osteoconductive properties of the implant surface, and to potentially decrease ionic exchange between the implant substrate and the peri-implant tissues [1].

Despite the utilization of a partially crystalline target (PSHA) and the abalation of target material into a range of nanometer sized clusters, the thin-film XRD spectra showed no evidence of HA or any other Ca- and P-based crystalline phase (only an alpha Ti peak at 35.5 degrees 2-theta was observed) (Fig. 2c). This indicates that the coatings were primarily of amorphous microstructure with Ca/P ratios higher than crystalline HA (1.677) (Fig. 2a). This result is in agreement with previous studies which demonstrated that crystalline content in sputtering systems typically require subsequent heat treatment to achieve Ca- and P-phases long range ordering [10, 28].

Previous in vitro dissolution studies indicate that high dissolution rates are expected [10] with the thin, primarily amorphous microstructure sputtered coating created in the present study,. Thus, the release of Ca and P after implantation would likely not be sustained levels over longer periods of time (total coating dissolution). Interfacial electrochemical properties may decrease the device biocompatibility. However, studies concerning the in vivo dissolution of coating thicknesses ranging from 100 nm to 4 μm have shown, that after several weeks, carbonitic apatite existed with all thin films in vivo [33, 34]. Thus, it is possible that the release of Ca and P may have substantially different kinetics in vivo compared to in vitro, and the thin coatings like the one investigated in the present study may not completely dissolve over longer periods of time as has been observed with PSHA [26].

EIS has been established as a powerful, non-destructive method for the characterization of titanium alloys [35–37] and bioactive ceramic coated titanium alloys' [38, 39] surfaces. In the present study, PBS solution (Table 1) was selected as the electrochemical testing electrolyte in an attempt to better simulate the interaction between biofluids and surfaces following implantation [40, 41]. Figure 3 shows the Bode and Nyquist diagrams for the coated and uncoated Ti-6Al-4V alloy following 3 days of immersion in PBS solution.

As previously reported for Ti-6Al-4V [35–37] and thin sol-gel processed bioactive ceramic coatings on Ti-6Al-4V [38], the Bode phase angle diagrams showed highly capacitive results indicated by the phase angles near to −90° from medium to low frequencies (Fig. 3). The absence of the real component of impedance at low frequencies (in the range presented) and the corresponding

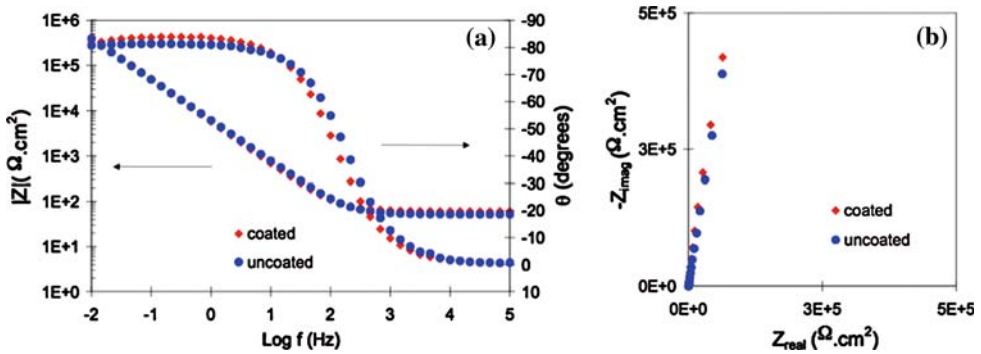

Fig. 3 EIS results for Ti-6Al-4V, coated or uncoated, after 3 days of immersion in naturally aerated PBS solution: (**a**) Bode phase angle and Z modulus and (**b**) Nyquist diagrams

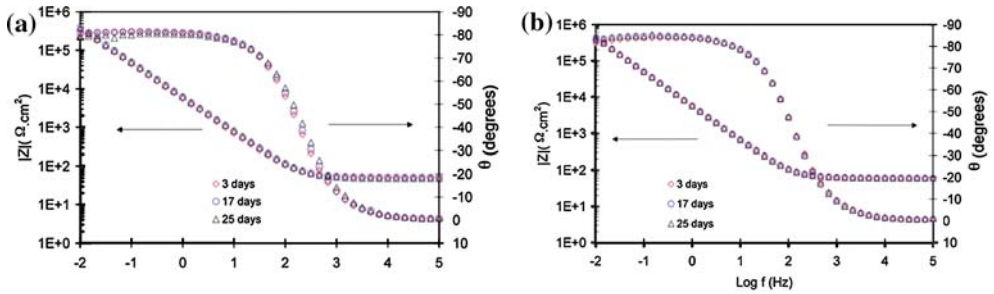

Fig. 4 (**a**) Bode diagrams obtained for the uncoated and coated (**b**) Ti-6Al-4V alloy as a function of time of immersion in PBS solution

absolute value of Z indicates a high charge-transfer resistance (corrosion resistance) [35–39]. The large plateau at this frequency range also suggests the interaction of more than one time constant as usually found for Ti alloys exposed to solutions that simulate body fluids [37].

The EIS diagrams shown in Fig. 4 depict the temporal electrochemical behavior of uncoated and coated surfaces in PBS solution. The results confirm that both coated and uncoated surfaces were stable in the test solution with these highly protective characteristics maintained throughout the 25 days of PBS immersion.

The polarization curves presented in Fig. 5 showed very low current densities (extrapolated from the linear region of the cathodic curve to the corrosion potential, E_{corr}). The densities were in the order of 10^{-8} A/cm^2, at the corrosion potential (E_{corr}) of the uncoated Ti-6Al-4V specimens, which is commonly observed for passive materials with very protective surface films (Table 2) [35, 37, 38]. Slightly lower current densities and nobler corrosion potential were associated with the coated Ti-6Al-4V specimens. The slight current density difference between coated and uncoated surfaces along with the nobler E_{corr} with respect to SCE for the coated surface suggest a slight beneficial effect of the coating on corrosion resistance [36].

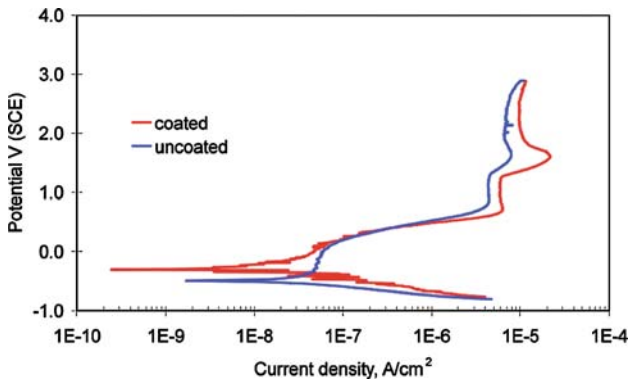

Fig. 5 Potentiodynamic polarization curves for Ti-6Al-4V alloy obtained for coated and uncoated specimens after 3 days immersion in PBS NaCl solution, at 25°C

Despite the increase in current density as the potential was increased to approximately 0.8 V (SCE), current density was essentially independent of the potential value up to approximately 1.3 V (SCE) for both uncoated and coated surfaces. This, suggests the establishment of a passive region with current densities in the range of 10^{-5} to 10^{-6} A/cm^2, typically observed in surfaces with a passive character (Fig. 5) [35, 37, 38]. The current density in this passive range was approximately 4×10^{-6} A/cm^2 and 6×10^{-6} A/cm^2 for the uncoated and coated surfaces, respectively. In this potential range, the coating had no substantial effect on the corrosion resistance of the substrate. At a potential value of approximately 1.3 V (SCE), the current density increased for both surfaces with a higher magnitude increase for the coated surface. For titanium alloys in general, current density increase at potentials around 1.3 V (SCE) has been associated withe first passive film breakdown and subsequent repassivation, by secondary passive film formation, or by formation of Ti_2O_5 [33]. The higher current density associated with the coated surfaces may result from porosity within the coating structure induced by polarization [38]. At potentials around 1.9 V (SCE), the current was again stabilized, suggesting the setting up of another passive region for both coated and uncoated surfaces.

According to the potentiodynamic polarization curves generated under PBS solution, the bioactive ceramic coated surfaces presented corrosion resistance comparable to uncoated surfaces. While insight regarding the remarkably similar corrosion resistance between the uncoated and coated Ti-6Al-4V disks was obtained through our in vitro

Table 2 Average values of corrosion potential (E_{corr}), corrosion current density (i_{corr}) and their respectie standard deviations obtained for Ti-6Al-4V, coated and uncoated, after 3 days of immersion in PBS solution ($n = 3$)

Ti-6Al 4V	E_{corr}		i_{corr}	
	mV	Standard deviation	nA/cm^2	Standard deviation
Coated	−270	(50)	30	(14)
Uncoated	310	(250)	40	(21)

testing set up, implant surface characteristics are dynamically changed immediately after implantation [2]. For the case of the uncoated Ti-6Al-4V surface, an increase in the oxide layer is expected to occur with time from implantation [2], whereas thick PSHA coated implant surfaces are known to promote apatitic depositions from interactions with the host biofluids [2]. In the case of substantially thinner bioactive ceramic coating, studies have shown apatitic depositions similar to those observed for PSHA also occur in vivo [33, 34]. For the thin Ca–P coatings described here it is possible that as implantation time elapses little to no coating will be present due to dissolution and/or bone remodeling [10, 15]. Thus, thin coating electrochemical properties may evolve towards characteristics either similar to or much more complex than uncoated Ti-6Al-4V surfaces. In order to investigate the in vivo evolution of these thin amorphous bioactive ceramic coatings, controlled animal studies providing implant retrievals at various implantation times must be performed and retrieved specimens characterized electrochemically.

4 Conclusion

Thin (400–700 nm) amorphous Ca- and P-based coatings with high Ca/P ratios were successfully sputtered on Ti-6Al-4V surfaces. A range of corrosion tests in PBS solution, found the thin bioactive ceramic coated surfaces to have corrosion resistance comparable to uncoated surfaces.

References

1. J.E. Lemons, Biomaterials, biomechanics, tissue healing, and immediate-function dental implants. J. Oral. Implantol. **30**, 318 (2004). doi:10.1563/0712.1
2. J.E. Davies, Bone bonding at natural and biomaterial surfaces. Biomaterials **28**, 5058 (2007). doi:10.1016/j.biomaterials.2007.07.049
3. T. Albrektsson, A. Wennerberg, Oral implant surfaces: Part 1—review focusing on topographic and chemical properties of different surfaces and in vivo responses to them. Int. J. Prosthodont. **17**, 536 (2004)
4. T. Albrektsson, A. Wennerberg, Oral implant surfaces: Part 2—review focusing on clinical knowledge of different surfaces. Int. J. Prosthodont. **17**, 544 (2004)
5. E. Eisenbarth, D. Velten, M. Muller, R. Thull, J. Breme, Biocompatibility of beta-stabilizing elements of titanium alloys. Biomaterials **25**, 5705 (2004). doi:10.1016/j.biomaterials.2004.01.021
6. E. Eisenbarth, D. Velten, K. Schenk-Meuser, P. Linez, V. Biehl, H. Duschner et al., Interactions between cells and titanium surfaces. Biomol. Eng. **19**, 243 (2002). doi:10.1016/S1389-0344(02)00032-1
7. T. Hanawa, M. Kaga, Y. Itoh, T. Echizenya, H. Oguchi, M. Ota, Cytotoxicities of oxides, phosphates and sulphides of metals. Biomaterials **13**, 20 (1992). doi:10.1016/0142-9612(92)90089-7
8. W.R. Lacefield, Hydroxyapatite coatings. Ann. N. Y. Acad. Sci. **523**, 72 (1988). doi:10.1111/j.1749-6632.1988.tb38501.x
9. W.R. Lacefield, Current status of ceramic coatings for dental implants. Implant. Dent. **7**, 315 (1998). doi:10.1097/00008505-199807040-00010
10. Y. Yang, K.H. Kim, J.L. Ong, A review on calcium phosphate coatings produced using a sputtering process—an alternative to plasma spraying. Biomaterials **26**, 327 (2005). doi:10.1016/j.biomaterials.2004.02.029
11. J.L. Ong, D.L. Carnes, K. Bessho, Evaluation of titanium plasma-sprayed and plasma-sprayed hydroxyapatite implants in vivo. Biomaterials **25**, 4601 (2004). doi:10.1016/j.biomaterials.2003.11.053
12. J. Lemons, F. Dietch-Misch, in *Biomaterials for Dental Implants*, ed. by C.E. Misch. Contemporary Implant Dentistry (Mosby Inc., Saint Louis, 1999), p. 271
13. J. Kay, Calcium phosphate coatings for dental implants. Dent. Clin. North Am. **36**, 1 (1992)
14. K.K.C. deGroot, J.G.C. Wolke, J.M. deBieck-Hogervorst, Plasma-sprayed coating of calcium phosphate, in *Handbook of Bioactive Ceramics, Calcium Phosphate and Hydroxyapatite Ceramics*, vol. II, ed. by T.H.L. Yamamuro, J. Wilson (CRC Press, Boca Raton, 1990), p. 17
15. Y.S. Park, K.Y. Yi, I.S. Lee, C.H. Han, Y.C. Jung, The effects of ion beam-assisted deposition of hydroxyapatite on the grit-blasted surface of endosseous implants in rabbit tibiae. Int. J. Oral Maxillofac. Implants **20**, 31 (2005)
16. P.G. Coelho, J.E. Lemons, IBAD nanothick bioceramic incorporation on metallic implants for bone healing enhancement. From physico/chemical characterization to in-vivo performance evaluation. Nanotech 2005, **1**, 316 (2005) ISBN, editor, Anaheim, CA
17. R.Z. LeGeros, S. Lin, R. Rohanizadeh, D. Mijares, J.P. LeGeros, Biphasic calcium phosphate bioceramics: preparation, properties and applications. J. Mater. Sci. Mater. Med. **14**, 201 (2003). doi:10.1023/A:1022872421333
18. J. Pan, C. Leygraf, D. Thierry, A.M. Ektessabi, Corrosion resistance for biomaterial applications of TiO2 films deposited on titanium and stainless steel by ion-beam-assisted sputtering. J. Biomed. Mater. Res. **35**, 309 (1997). doi:10.1002/(SICI)1097-4636(19970605)35:3<309::AID-JBM5>3.0.CO;2-L
19. J. Pan, D. Thierry, C. Leygraf, Electrochemical and XPS studies of titanium for biomaterial applications with respect to the effect of hydrogen peroxide. J. Biomed. Mater. Res. **28**, 113 (1994). doi:10.1002/jbm.820280115
20. J. Pan, D. Thierry, C. Leygraf, Hydrogen peroxide toward enhanced oxide growth on titanium in PBS solution: blue coloration and clinical relevance. J. Biomed. Mater. Res. **30**, 393 (1996). doi:10.1002/(SICI)1097-4636(199603)30:3<393::AID-JBM14>3.0.CO;2-L
21. P.G. Coelho, J.E. Lemons, Physico/chemical characterization and in vivo evaluation of nanothickness bioceramic depositions on alumina-blasted/acid-etched Ti-6Al-4 V implant surfaces. J. Biomed. Mater. Res. A. (2008)
22. J.P. LeGeros, R.Z. LeGeros, A. Burgess, B. Edwards, J. Zitelli, in *X-Ray Diffraction Method for the Quantitative Characterization of Calcium Phosphate Coatings*. ed. by E. Horowitz, J.A. Parr. Characterization and Performance of Calcium Phosphate Coatings for Implants, vol 1196 (STP: ASTM, Philadelphia, 1994), p. 33
23. Y.C. Tsui, C. Doyle, T.W. Clyne, Plasma sprayed hydroxyapatite coatings on titanium substrates. Part 2: optimisation of coating properties. Biomaterials **19**, 2031 (1998). doi:10.1016/S0142-9612(98)00104-5
24. R.J. Furlong, J.F. Osborn, Fixation of hip prostheses by hydroxyapatite ceramic coatings. J. Bone Joint Surg. Br. **5**, 741 (1991)

25. R.Z. LeGeros, Properties of osteoconductive biomaterials: calcium phosphates. Clin. Orthop. Relat. Res. 81 (2002). doi:10.1097/00003086-200202000-00009
26. J.L. Ong, K. Bessho, D.L. Carnes, Bone response to plasma-sprayed hydroxyapatite and radiofrequency-sputtered calcium phosphate implants in vivo. Int. J. Oral Maxillofac. Implants **17**, 581 (2002)
27. T.W. Bauer, J. Schils, The pathology of total joint arthroplastyI. Mechanisms of implant fixation. Skeletal Radiol. **28**, 423 (1999). doi:10.1007/s002560050541
28. J.L. Ong, L.C. Lucas, Post-deposition heat treatments for ion beam sputter deposited calcium phosphate coatings. Biomaterials **15**, 337 (1994). doi:10.1016/0142-9612(94)90245-3
29. J.L. Ong, C.W. Prince, L.C. Lucas, Cellular response to well-characterized calcium phosphate coatings and titanium surfaces in vitro. J. Biomed. Mater. Res. **29**, 165 (1995). doi:10.1002/jbm.820290205
30. A.E. Porter, L.W. Hobbs, V.B. Rosen, M. Spector, The ultra-structure of the plasma-sprayed hydroxyapatite-bone interface predisposing to bone bonding. Biomaterials **23**, 725 (2002). doi:10.1016/S0142-9612(01)00177-6
31. K. Soballe, S. Overgaard, E.S. Hansen, H. Brokstedt-Rasmussen, M. Lind, C. Bunger, A review of ceramic coatings for implant fixation. J. Long. Term. Eff. Med. Implants. **9**, 131 (1999)
32. L. Sun, C.C. Berndt, K.A. Gross, A. Kucuk, Material fundamentals and clinical performance of plasma-sprayed hydroxyapatite coatings: a review. J. Biomed. Mater. Res. **58**, 570 (2001). doi:10.1002/jbm.1056
33. J.G. Wolke, K. de Groot, J.A. Jansen, In vivo dissolution behavior of various RF magnetron sputtered Ca–P coatings. J. Biomed. Mater. Res. **39**, 524 (1998). doi:10.1002/(SICI)1097-4636(19980315)39:4<524::AID-JBM3>3.0.CO;2-L
34. J.G. Wolke, J.P. van der Waerden, H.G. Schaeken, J.A. Jansen, In vivo dissolution behavior of various RF magnetron-sputtered Ca–P coatings on roughened titanium implants. Biomaterials **24**, 2623 (2003). doi:10.1016/S0142-9612(03)00067-X
35. J.E.G. Gonzalez, J.C. Mirza-Rosca, Study of the corrosion behavior of titanium and some of its alloys for biomedical and dental applications. J. Electroanal. Chem. **471**, 109 (1999). doi:10.1016/S0022-0728(99)00260-0
36. R.W. Hsu, C. Yang, C. Huang, Y. Chen, Electrochemical corrosion properties of Ti-6Al-4 V implant alloy in the biological environment. Mater. Sci. Eng. A **380**, 100 (2004). doi:10.1016/j.msea.2004.03.069
37. J. Pan, D. Thierry, C. Leygraf, Electrochemical impedance spectroscopy study of the passive oxide film on titanium for implant application. Electrochim. Acta **41**, 1143 (1996). doi:10.1016/0013-4686(95)00465-3
38. M.C. Advincula, D. Petersen, F. Rahemtulla, R. Advincula, J.E. Lemons, Surface analysis and biocorrosion properties of nano-structured surface sol-gel coatings on Ti6Al4 V titanium alloy implants. J. Biomed. Mater. Res. B Appl. Biomater. **80**, 107 (2007). doi:10.1002/jbm.b.30575
39. I.C. Lavos-Valereto, I. Costa, S. Wolynec, The electrochemical behavior of Ti-6Al-7Nb alloy with and without plasma-sprayed hydroxyapatite coating in Hank's solution. J. Biomed. Mater. Res. **63**, 664 (2002). doi:10.1002/jbm.10351
40. P. Tengvall, A. Askendal, I. Lundstrom, H. Elwing, Studies of surface activated coagulation: antisera binding onto methyl gradients on silicon incubated in human plasma in vitro. Biomaterials **13**, 367 (1992). doi:10.1016/0142-9612(92)90042-M
41. P. Tengvall, I. Lundstrom, L. Sjoqvist, H. Elwing, L.M. Bjursten, Titanium-hydrogen peroxide interaction: model studies of the influence of the inflammatory response on titanium implants. Biomaterials **10**, 166 (1989). doi:10.1016/0142-9612(89)90019-7